Vietnam Journal of Science and Technology ***61*** *(4) (2023) 692-707*

doi:10.15625/2525-2518/17507

Dynamics of functionally graded beams carrying a moving load with influence of porosities and partial foundation support

Vu Thi An Ninh

University of Transport and Communications, 3 Cau Giay, Dong Da, Ha Noi, Viet Nam

Email: *vuthianninh@utc.edu.vn*

Received: 13 September 2022; Accepted for publication: 11 May 2023

Abstract. The novelty of the present work is to study the simultaneous influence of porosities and partial Pasternak foundation support on dynamics of functionally graded (FG) beams carrying a moving load. The beams are made from an open-cell steel foam with symmetric and asymmetric porosity distributions in the thickness direction. Based on a refined third-order shear deformation theory, a two-node beam element with ten degrees of freedom is derived and employed to construct the discretized equation of motion for the beams. Dynamic characteristics, including the time histories for mid-span deflection, dynamic magnification factor (DMF) and the stress distribution, are computed with the aid of the Newmark method. The numerical result reveals that the foundation supporting length has an important role on the dynamics of the beams, and the dependence of the DMF upon the porosity coefficient is governed by the foundation supporting length. It is also found that the asymmetric porosity distribution has more impact on the dynamic response of the beams than the symmetric one does, and the difference between the DMFs obtained from the two porosity distributions is more significant for the beam with a higher porosity coefficient. The effects of the porosities, the foundation support and the moving load velocity on the dynamic behavior of the beams are examined in detail and highlighted.

Keywords: FG beam, porosities, partial foundation support, refined shear deformation theory, moving load, dynamic analysis.

Classification numbers: 5.4.2, 5.4.5.

1. INTRODUCTION

Dynamics of beams made of functionally graded (FG) materialshas been extensively carried out since the invention of the materials by Japanese researchers in 1984 [1]. It has been reported that the dynamic characteristics of FG beams are greatly influenced by the material gradation in the beam thickness. Şimşek and Kocatürk [2] employed the polynomials to approximate the displacement field in the dynamic analysis of an FG Euler-Bernoulli beam under a moving harmonic load. Their study revealed that the material gradation has significantly altered the dynamic deflections and stresses of the beam. The method was then extended by

Şimşek [3] to analysis of shear deformable FG beams excited by a moving load. Rayleigh-Ritz method was used in conjunction with the differential quadrature method by Khalili *et al.* [4] to study vibration of FG Euler-Bernoulli beams with a moving load. Rajabi *et al.* [5] investigated the influence of a power-law thickness gradation of material properties on dynamics of the FG Euler-Bernoulli beam excited by a moving oscillator. Using the Petrov-Galerkin approach, they transferred the system of fourth-order differential equations of motion to a system of second-order ordinary differential equations, and then computed dynamic response using the Runge-Kutta method. The influence of temperature on the dynamics of axially FG Timoshenko beams under a moving harmonic load was studied by Wang and Wu [6]. They found that the dynamic deflections are increased by increasing the temperature. Songsuwan *et al.* [7] used the Ritz method to study the vibration of FG sandwich Timoshenko beams on a Pasternak foundation under a moving harmonic load. The authors concluded that the material gradation and the layer thickness ratio of the beams play an important role on the dynamic behavior of the beams.

The finite element method was widely used by researchers to study dynamics of FG beams with a moving load. Gan *et al*. [8] derived a two-node Timoshenko beam element for computing dynamic response of nonuniform axially FG beams. The solution of the equilibrium equations of a beam segment has been employed to interpolate the displacement field to improve the efficiency of the element. Esen [9, 10], Esen *et al*. [11] studied dynamics of FG Timoshenko beams under a moving mass using the simple finite element procedures. The power-law or sigmoid variation was assumed for the beam material properties, and the influence of the foundation support and the temperature rise on the dynamics was considered. Nguyen *et al*. [12, 13] derived the finite element formulations for studying the vibration of FG and FG sandwich Timoshenko beams carrying a moving load, respectively. The material properties were considered to be graded in both the axial and transverse directions by the power gradation laws. The works were then extended by the authors to dynamic analysis of the FG sandwich and inclined FG sandwich beams under a moving mass [14, 15]. The beams considered in the work are made from three constituent materials with material properties being graded in both the longitudinal and thickness directions by the power laws.

Due to the large difference in the solidification temperature of the constituent materials, micro-voids and porosities are often occurred during the fabrication of FG materials. Investigations on the mechanical behavior of FG structures, taking into account the influence of mirco-voids and porosities, therefore are important. Wattanasakulpong and Ungbhakorn [16] assumed a uniform distribution of porosities in the beam cross-section in their linear and nonlinear free vibration analysis of power-law FG beams with elastic boundary conditions. They concluded that the increase of porosity volume results in a lower linear fundamental frequency, but a higher nonlinear frequency ratio. Using the Ritz method, Chen *et al*. [17] studied vibration of porous FG Timoshenko beams with porosity distribution in the beam thickness by trigonometric functions. Their findings showed that the asymmetric porosity distribution has a more significant effect on the frequencies and dynamic response of the beams than the symmetric porosity distribution does. Ebrahimi and Jafari [18 - 20], Ebrahimi *et al.* [21] adopted various shear deformation theories to derive the governing equations for thermomechanical vibration analysis of FG porous beams. Their findings dshowed that the even porosity distribution has a more remarkable impact on natural frequencies than the uneven one does. Based on a hyperbolic theory, Atmane *et al*. [22] derived differential equations of motion for free vibration analysis of FG porous beams on elastic foundation. The shift of the neutral axis from the mid-plane considered in the derivation leads to the equations without a coupling term. Dynamics of FG porous sandwich beams with three different types of porosity distributions subjected to a pulse load was investigated by Akbaş *et al*. [23], using a finite element

formulation. Rayleigh-Ritz method was used with Navier technique by Jena *et al*. [24] to examine the influence of porosities on the vibration of FG beams on the Kerr elastic foundation.

As previously reported by Vu *et al*. [25], the dynamics of FG beams partially supported by an elastic foundation is considerably different from that of the beams without or full foundation support. Motivated by this fact, the simultaneous influence of the porosities and partial support by a Pasternak foundation on the dynamics of FG beams carrying a moving load is investigated in the present work. The beams are considered to be made from open-cell steel foam with two types of porosity distribution, the symmetric and asymmetric distributions as introduced in [17]. A refined third-order shear deformation theory, in which the transverse displacement is split into bending and shear parts, is adopted to model the beams. A finite element formulation is derived and employed to construct the discretized equation of motion for the beams. Dynamic responses of the beams, including the time histories for mid-span deflections, dynamic magnification factors and stress distribution, are computed with the aid of the Newmark method. The effects of the material distribution, porosities, the foundation support as well as the moving load velocity on the dynamic behavior of the beams are studied in detail and highlighted.

2. PROBLEM STATEMENT

A simply supported FG porous beam with length L, a rectangular cross-section ($b \times h$), partially supported by a Pasternak elastic foundation, as shown in Figure 1, is considered. The foundation is represented by Winkler springs with stiffness k_w and a shear layer with stiffness k_s. In this Figure, $\alpha_F = L_F/L$ is the foundation supporting parameter, and it is defined by the ratio between the foundation supporting part (L_F) and the total beam length (L).

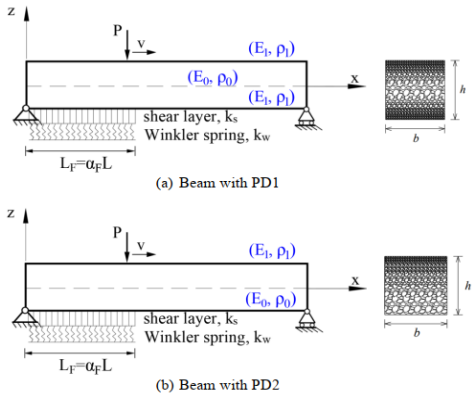

Figure 1. FG beam with porosities partially supported by Pasternak foundation under a moving load.

Two different porosity distributions through the beam thickness, namely symmetric porosity distribution 1 (referred to as PD1) as shown in Figure 1a and asymmetric porosity distribution 2 (referred to as PD2) as depicted in Figure 1b, are considered. The Cartesian coordinate system (x, y, z) in Figure 1 is chosen such that the (x, y) plane is on the beam mid-plane, and the z-axis is perpendicular to the mid-plane and it directs upward. The beam is assumed to be under the action of a load P, moving with a constant velocity v from the left end to the right end of the beam. It is assumed that the moving load P is always in contact with the beam during its motion on the beam.

The effective material properties of the beam, such as the Young's modulus E_f and the mass density ρ_f, are defined as follows [17, 26]

- For PD1:

$$E_f = E_1\left[1-e_0\cos\left(\frac{\pi z}{h}\right)\right], \quad \rho_f = \rho_1\left[1-e_m\cos\left(\frac{\pi z}{h}\right)\right] \tag{1}$$

- For PD2:

$$E_f = E_1\left[1-e_0\cos\left(\frac{\pi z}{2h}+\frac{\pi}{4}\right)\right], \quad \rho_f = \rho_1\left[1-e_m\cos\left(\frac{\pi z}{2h}+\frac{\pi}{4}\right)\right] \tag{2}$$

In Eqs. (1) and (2), E_1 and ρ_1 are, respectively, the maximum values of Young's modulus and mass density of constituent materials of the FG beam; e_0 is the porosity coefficient, and e_m is the mass density coefficient. The values of e_0 and e_m are defined as [17]

$$e_0 = 1-\frac{E_0}{E_1}, \quad e_m = 1-\frac{\rho_0}{\rho_1}, \quad (0 < e_0, e_m < 1) \tag{3}$$

where E_0 and ρ_0 are, respectively, the minimum values of Young's modulus and mass density. In practice, Young's modulus and density are not independent to each other, e.g. for a typical open-cell metal foam, they have the following relationship [17]

$$\frac{E_0}{E_1} = \left(\frac{\rho_0}{\rho_1}\right)^2, \tag{4}$$

The relationship between e_m and e_0, obtained from Equations (3) and (4), is of the form

$$e_m = 1-\sqrt{1-e_0} \tag{5}$$

It is evident from Equation (1) that Young's modulus and the mass density of the PD1 beam attain maximum values at the outermost surfaces, while their minimum values occur at the mid-plane. For the PD2 beam, as seen from (2), the maximum and minimum values of these effective properties are at the top and bottom surfaces, respectively.

3. MATHEMATICAL FORMULATION

According to the refined third-order shear deformation theory proposed by Thai and Kim in [27], the displacements in the x and z directions, $u_1(x,z,t)$ and $u_3(x, z, t)$, are respectively given by

$$\begin{aligned} u_1(x,z,t) &= u(x,t) - z w_{b,x}(x,t) + f(z)\, w_{s,x}(x,t) \\ u_3(x,z,t) &= w_b(x,t) + w_s(x,t) \end{aligned} \tag{6}$$

where $u(x,t)$ is the axial displacement of the point on the beam mid-plane; $w_b(x,t)$ and $w_s(x,t)$ are, respectively, the bending and shear components of the transverse displacement; t is the time variable, and

$$f(z) = -\frac{4z^3}{3h^2} \tag{7}$$

is the shape function for the shear component. In Equation (6) and hereafter, a subscript comma is used to denote the derivative with respect to the variable which follows.

The axial strain (ε_{xx}) and shear strain (γ_{xz}) resulted from Equation (6) are as follows

$$\varepsilon_{xx} = u_{,x} - z w_{b,xx} + f(z)\, w_{s,xx}, \quad \gamma_{xz} = g(z)\, w_{s,x} \tag{8}$$

with $g\ \ z\ =1+\ f_{,z}$.

The stresses associated with the strain components in Equation (8) for the linear material are of the forms

$$\sigma_{xx} = E_f \varepsilon_{xx}, \quad \tau_{xz} = G_f \gamma_{xz} \tag{9}$$

where σ_{xx} and τ_{xz} are, respectively, the axial and shear stresses; $G_f = \dfrac{E_f}{2(1+\upsilon)}$ is the effective shear modulus; υ is Poisson's ratio, which assumed to be unchanged in the thickness direction.

The elastic strain energy due to the beam deformation (U_B) is given by

$$U_B = \frac{1}{2}\int_0^L \int_A \ \sigma_{xx}\varepsilon_{xx} + \tau_{xz}\gamma_{xz}\ \ dAdx \tag{10}$$

where $A = b \times h$ is the beam cross-sectional area.

Substituting Equations (8) and (9) into Equation (10), one gets

$$U_B = \frac{1}{2}\int_0^L \ A_{11}u_{,x}^2 - 2A_{12}u_{,x}w_{b,xx} + A_{22}w_{b,xx}^2 + 2B_{11}u_{,x}w_{s,xx} - 2B_{12}w_{b,xx}w_{s,xx} + B_{22}w_{s,xx}^2 + D_{11}w_{s,x}^2\ \ dx \tag{11}$$

where the beam rigidities A_{11}, A_{12}, A_{22}, B_{11}, B_{12}, B_{22} and D_{11} are defined as follows

$$\begin{aligned} A_{11}, A_{12}, A_{22}\ &= b\int_{-\frac{h}{2}}^{\frac{h}{2}} E_f\ \ 1, z, z^2\ \ dz\,, \quad D_{11} = b\int_{-\frac{h}{2}}^{\frac{h}{2}} G_f g^2\ \ z\ \ dz, \\ B_{11}, B_{12}, B_{22}\ &= b\int_{-\frac{h}{2}}^{\frac{h}{2}} E_f\left[1, z, f\ \ z\ \right] f\ \ z\ \ dz\,, \end{aligned} \tag{12}$$

The strain energy stored in the elastic foundation (U_F) can be expressed as

$$U_F = \frac{b}{2}\int_0^{L_F} \ k_w u_3^2 + k_s u_{3,x}^2\ dx = \frac{b}{2}\int_0^{L_F}\left[k_w\ \ w_b + w_s\ ^2 + k_s\ \ w_{b,x} + w_{s,x}\ ^2\right]dx \tag{13}$$

The kinetic energy of the beam (T) resulted from Eq. (6) is of the form

$$T = \frac{1}{2}\int_0^L \int_A \rho_f\ \ \dot{u}_1^2 + \dot{u}_3^2\ dAdx \tag{14}$$

where an over dot is used to denote the derivative with respect to the time variable t. Substituting Eq. (6) into Eq. (14), one gets

$$T = \frac{1}{2}\int_0^L \ I_{11}\left[\dot{u}^2 + \ \dot{w}_b + \dot{w}_s\ ^2\right] - 2I_{12}\dot{u}\dot{w}_{b,x} + I_{22}\dot{w}_{b,x}^2 + 2J_{11}\dot{u}\dot{w}_{s,x} - 2J_{12}\dot{w}_{b,x}\dot{w}_{s,x} + J_{22}\dot{w}_{s,x}^2\ \ dx \tag{15}$$

where I_{11}, I_{12}, I_{22}, J_{11}, J_{12} and J_{22} are the mass moments of the beam, defined as

$$I_{11}, I_{12}, I_{22}\ = b\int_{-\frac{h}{2}}^{\frac{h}{2}} \rho_f\ \ 1, z, z^2\ \ dz\,, \quad J_{11}, J_{12}, J_{22}\ = b\int_{-\frac{h}{2}}^{\frac{h}{2}} \rho_f\left[1, z, f\ \ z\ \right] f\ \ z\ \ dz \tag{16}$$

Finally, the potential energy (V) of the moving load P is given by

$$V = -\int_0^L P u_3 \delta\ x_P - vt\ dx = -\int_0^L P\ w_b + w_s\ \delta\ x_P - vt\ dx \tag{17}$$

where $\delta(.)$ is the Dirac delta function, and x_P is the current abscissa of the moving load, measured from the left end of the beam.

Differential equations of motion for the beam can be obtained by applying Hamilton's principle to Eqs. (11), (13), (15) and (17). However, a closed-form solution for such equations is hardly to obtain. A finite element formulation is derived in the next section to construct the discretized equation of motion and to obtain the vibration characteristics of the beam.

4. SOLUTION METHOD

A two-node beam element formulation is formulated in this Section to construct the discretized equation of motion for the beam. To this end, the beam is assumed to be divided into a number of beam elements with length *l*. The vector of nodal displacements **d** for the element contains ten components as

$$\underset{10\times1}{\mathbf{d}} = \begin{bmatrix} \mathbf{d}_u & \mathbf{d}_{w_b} & \mathbf{d}_{w_s} \end{bmatrix}^T \tag{18}$$

with $\mathbf{d}_u$, $\mathbf{d}_{wb}$, $\mathbf{d}_{ws}$ are, respectively, the vectors of nodal displacements for u, w_b, w_s, and they have the following forms

$$\mathbf{d}_u = \begin{bmatrix} u_1 & u_2 \end{bmatrix}^T,\ \mathbf{d}_{w_b} = \begin{bmatrix} w_{b1} & w_{b1,x} & w_{b2} & w_{b2,x} \end{bmatrix}^T,\ \mathbf{d}_{w_s} = \begin{bmatrix} w_{s1} & w_{s1,x} & w_{s2} & w_{s2,x} \end{bmatrix}^T \tag{19}$$

where ui, w_{bi}, $w_{bi,x}$, w_{si} and $w_{si,x}$ (i = 1, 2) are the values of u, w_b, $w_{b,x}$, w_s and $w_{s,x}$ at the node i, respectively. The superscript 'T' in the above equations and hereafter is used to denote the transpose of a vector or a matrix.

The axial and transverse displacements are interpolated from their nodal values as follows

$$u = \mathbf{N}\mathbf{d}_u,\quad w_b = \mathbf{H}\mathbf{d}_{w_b},\quad w_s = \mathbf{H}\mathbf{d}_{w_s} \tag{20}$$

where **N** and **H** are the shape function matrices with the following forms

$$\mathbf{N} = \begin{bmatrix} N_1 & N_2 \end{bmatrix},\quad \mathbf{H} = \begin{bmatrix} H_1 & H_2 & H_3 & H_4 \end{bmatrix} \tag{21}$$

In the above formula, N_i (i=1,2) are linear interpolation functions, and H_i (i=1,…,4) are cubic Hermite polynomials.

Using the above interpolations, the strain energy of the beam in Equation (11) can be written as

$$U_B = \frac{1}{2}\sum^{neB} \mathbf{d}^T \mathbf{k}_B \mathbf{d} \tag{22}$$

where *neB* is the total number of elements used to discretize the beam; and $\mathbf{k}_B$ is the beam element stiffness matrix, which can be split into sub-matrices as

$$\underset{10\times10}{\mathbf{k}_B} = \begin{bmatrix} \mathbf{k}_{aa}^B & \mathbf{k}_{ab}^B & \mathbf{k}_{as}^B \\ \mathbf{k}_{ab}^{B\ T} & \mathbf{k}_{bb}^B & \mathbf{k}_{bs}^B \\ \mathbf{k}_{as}^{B\ T} & \mathbf{k}_{bs}^{B\ T} & \mathbf{k}_{ss}^B \end{bmatrix} \tag{23}$$

In the above equation, the sub-matrices $\mathbf{k}_{aa}^B$, $\mathbf{k}_{bb}^B$ and $\mathbf{k}_{ss}^B$ are, respectively, the element stiffness matrices stemming from the axial stretching, bending and shear deformation, and they have the following forms

$$\underset{2\times2}{\mathbf{k}_{aa}^{B}}=\int_{0}^{l}\mathbf{N}_{,x}^{T}A_{11}\mathbf{N}_{,x}dx,\quad \underset{4\times4}{\mathbf{k}_{bb}^{B}}=\int_{0}^{l}\mathbf{H}_{,xx}^{T}A_{22}\mathbf{H}_{,xx}dx,\quad \underset{4\times4}{\mathbf{k}_{ss}^{B}}=\int_{0}^{l}\left(\mathbf{H}_{,xx}^{T}B_{22}\mathbf{H}_{,xx}+\mathbf{H}_{,x}^{T}D_{11}\mathbf{H}_{,x}\right)dx \quad (24)$$

and $\underset{2\times4}{\mathbf{k}_{ab}^{B}}$, $\underset{2\times4}{\mathbf{k}_{as}^{B}}$ and $\underset{4\times4}{\mathbf{k}_{bs}^{B}}$ are, respectively, the axial stretching-bending, axial stretching-shear, bending-shear coupling matrices for the element and they have the following forms

$$\underset{2\times4}{\mathbf{k}_{ab}^{B}}=-\int_{0}^{l}\mathbf{N}_{,x}^{T}A_{12}\mathbf{H}_{,xx}dx,\quad \underset{2\times4}{\mathbf{k}_{as}^{B}}=\int_{0}^{l}\mathbf{N}_{,x}^{T}B_{11}\mathbf{H}_{,xx}dx,\quad \underset{4\times4}{\mathbf{k}_{bs}^{B}}=-\int_{0}^{l}\mathbf{H}_{,xx}^{T}B_{12}\mathbf{H}_{,xx}dx \quad (25)$$

The strain energy U_F in Eq. (13) can also be written in a matrix form as

$$U_F=\frac{1}{2}\sum^{ne_F}\mathbf{d}^{T}\mathbf{k}_{F}\mathbf{d} \quad (26)$$

where ne_F is the number of elements used to discretize the foundation; $\mathbf{k}_F$ is the element foundation stiffness matrix with the following form

$$\underset{10\times10}{\mathbf{k}_{F}}=\begin{bmatrix}\mathbf{0} & \mathbf{0} & \mathbf{0}\\ \mathbf{0} & \mathbf{k}_{bb}^{F} & \mathbf{k}_{bs}^{F}\\ \mathbf{0} & \mathbf{k}_{bs}^{F\ T} & \mathbf{k}_{ss}^{F}\end{bmatrix} \quad (27)$$

where

$$\underset{4\times4}{\mathbf{k}_{bb}^{F}}=\underset{4\times4}{\mathbf{k}_{ss}^{F}}=\underset{4\times4}{\mathbf{k}_{bs}^{F}}=b\int_{0}^{l}\left(\mathbf{H}^{T}k_{w}\mathbf{H}+\mathbf{H}_{,x}^{T}k_{s}\mathbf{H}_{,x}\right)dx \quad (28)$$

The total stiffness matrix ($\mathbf{k}$) for the element with the foundation support is as follows

$$\mathbf{k}=\mathbf{k}_{B}+\mathbf{k}_{F} \quad (29)$$

for the element without the foundation support, the matrix $\mathbf{k}$ is simply given by $\mathbf{k} = \mathbf{k}_B$.

Similarly, the kinetic energy of the beam in Eq (15) can be written in the following form

$$T=\frac{1}{2}\sum^{neB}\dot{\mathbf{d}}^{T}\mathbf{m}\dot{\mathbf{d}} \quad (30)$$

where the element mass matrix of the beam $\mathbf{m}$ with the following sub-matrix form

$$\underset{10\times10}{\mathbf{m}}=\begin{bmatrix}\mathbf{m}_{aa} & \mathbf{m}_{ab} & \mathbf{m}_{as}\\ \mathbf{m}_{ab}^{\ T} & \mathbf{m}_{bb} & \mathbf{m}_{bs}\\ \mathbf{m}_{as}^{\ T} & \mathbf{m}_{bs}^{\ T} & \mathbf{m}_{ss}\end{bmatrix} \quad (31)$$

with

$$\begin{aligned}&\underset{2\times2}{\mathbf{m}_{aa}}=\int_{0}^{l}\mathbf{N}^{T}I_{11}\mathbf{N}dx,\quad \underset{4\times4}{\mathbf{m}_{bb}}=\int_{0}^{l}\left(\mathbf{H}^{T}I_{11}\mathbf{H}+\mathbf{H}_{,x}^{T}I_{22}\mathbf{H}_{,x}\right)dx,\\ &\underset{4\times4}{\mathbf{m}_{ss}}=\int_{0}^{l}\left(\mathbf{H}^{T}I_{11}\mathbf{H}+\mathbf{H}_{,x}^{T}J_{22}\mathbf{H}_{,x}\right)dx,\quad \underset{4\times4}{\mathbf{m}_{bs}}=\int_{0}^{l}\left(\mathbf{H}^{T}I_{11}\mathbf{H}-\mathbf{H}_{,x}^{T}J_{12}\mathbf{H}_{,x}\right)dx\\ &\underset{2\times4}{\mathbf{m}_{ab}}=-\int_{0}^{l}\mathbf{N}^{T}I_{12}\mathbf{H}_{,x}dx,\ \underset{2\times4}{\mathbf{m}_{as}}=\int_{0}^{l}\mathbf{N}^{T}J_{11}\mathbf{H}_{,x}dx,\end{aligned} \quad (32)$$

The matrix form for the potential energy in Equation (17) is as follows

$$V = -\sum_{}^{neB} \mathbf{d}^T \mathbf{f}_P \tag{33}$$

where $\mathbf{f}_P$ is the time-dependent element nodal load vector caused by the moving load P, and it has the form

$$\underset{10\times 1}{\mathbf{f}_P} = P\left[\mathbf{0} \quad \mathbf{H}^T \quad \mathbf{H}^T\right]^T_{\bar{x}_P} \tag{34}$$

the notation $.\,_{\bar{x}_P}$ in Equation (34) means that the quantity [.] is evaluated at $\bar{x}_P$ -the current abscissa of the load P, measured from the left node of the element.

The discretized equation of motion for vibration analysis of the beam in case of neglecting the damping effect can be written in the following form

$$\mathbf{M}\ddot{\mathbf{D}} + \mathbf{K}\mathbf{D} = \mathbf{F} \tag{35}$$

where $\mathbf{D}$ and $\ddot{\mathbf{D}}$ are, respectively, the global vectors of nodal displacements and accelerations; $\mathbf{M}$, $\mathbf{K}$ and $\mathbf{F}$ are, respectively, the global matrices and vector obtained by respectively assembling the matrices $\mathbf{m}$, $\mathbf{k}$ and vector $\mathbf{f}_P$ over the elements. Equation (35) can be solved by the direct integration Newmark method. The average acceleration method, which ensures the unconditional convergence of the numerical solution [28] is adopted herein.

5. NUMERICAL INVESTIGATION

The influence of porosities and the partial foundation support on dynamics of a simply supported FG beam under the moving load is numerically studied in this section. The beam is made from the open-cell steel foam with E_1 = 200 GPa, ρ_1 = 7850 kg/m^3, ν = 1/3 [17]. The geometrical parameters of the beam used for calculation are as follows: h = 1 m, b = 0.5 m, and various values of the aspect ratio L/h. The non-dimensional parameters for dynamic magnification factor (DMF), foundation stiffness parameters k_1 and k_2 are introduced as follows

$$\text{DMF} = \max\left[\frac{w\ L/2,t}{w_{st}}\right], k_1 = \frac{k_w L^4}{E_1 I}, k_2 = \frac{k_s L^2}{E_1 I} \tag{36}$$

where $w_{st} = PL^3/48E_1I$ is the static deflection of the beam made from material with elastic modulus E_1 under a load P at the mid-span.

5.1. Validation and convergence

Table 1. Convergence of the beam element in evaluating dynamic magnification factors of FG porous beam for L/h = 20, α_F = 0.5, (k_1, k_2) = (100,5), v = 50 (m/s) and PD1.

e_0	neB = 2	neB = 4	neB = 6	neB = 8	neB = 10	neB = 12
0.2	0.8779	0.8737	0.8731	0.8733	0.8733	0.8733
0.4	0.9375	0.9333	0.9320	0.9316	0.9316	0.9316
0.6	1.0090	1.0036	1.0014	1.0010	1.0009	1.0009
0.8	1.0926	1.0878	1.0860	1.0856	1.0853	1.0853

The accuracy and convergence of the derived beam element are verified in this sub-section. To this end, the convergence of the derived element in evaluating the dynamic magnification factor DMF of FG porous beam with symmetric porosity distribution is shown in Table 1 for L/h = 20, α_F = 0.5, (k_1, k_2) = (100,5), v = 50 (m/s) and various porosity coefficients. As observed from

this table, the convergence of the derived element is also achieved using ten elements, regardless of porosity coefficients. Because of this convergence result, ten elements are used for all the computations reported below.

In order to validate the derived element in assessing the dynamic response of the beam, Table 2 compares the DMFs of a power-law FG beam under a moving load obtained herein with the results using the differential quadrature method of Khalili *et al*. [4] and Song *et al*. [29]. The DMFs of the present paper, as seen from Table 2, are very close to that of the cited references, irrespective of the power-law index n and the moving load velocity v. It is noted that the Euler-Bernoulli beam theory was employed by Khalili *et al*. [4], while the Kirchhoff plate theory was adopted by Song *et al*. [29].

Table 2. Comparison of dynamic magnification factor of FGM beam under a moving load.

v (m/s)	Source	n = 0.2	n = 0.5	n = 1	n = 2	n = 5	n = 10	n = 20
20	Ref. [4]	0.6252	0.7048	0.7706	0.8167	0.8903	0.9466	1.0009
	Ref. [29]	0.6128	0.6813	0.7552	0.8048	0.8686	0.9350	0.9968
	Present	0.6272	0.6946	0.7596	0.7995	0.8727	0.9449	1.0253
60	Ref. [4]	0.6872	0.7175	0.8155	0.9290	1.0433	1.1332	1.2218
	Ref. [29]	0.6923	0.7306	0.7812	0.8862	1.0069	1.1038	1.1932
	Present	0.6917	0.7275	0.7758	0.8803	1.0055	1.1123	1.2365
100	Ref. [4]	0.8260	0.9732	1.1155	1.2354	1.3491	1.4395	1.5291
	Ref. [29]	0.8091	0.9487	1.0826	1.1961	1.3175	1.4193	1.5153
	Present	0.8058	0.9453	1.0774	1.1905	1.3193	1.4299	1.5583

5.2. Numerical results

The influence of the foundation parameters, the porosity coefficient and the moving load velocity on the dynamics of the beam is studied in this sub-section. First of all, the dynamic magnification factors (DMFs) of the beam with the two types of porosity distribution are given in Table 3 for L/h = 15, v = 50 (m/s) and various values of the foundation parameters and the porosity coefficient. As can be seen from the table, the foundation supporting length and stiffness parameters as well as the porosity coefficient have a significant influence on the DMF of the beam.

Table 3. Dynamic magnification factors for L/h = 15 and v = 50 (m/s) and different porosity coefficients and foundation parameters.

		PD1				PD2		
(k_1, k_2)	α_F	e_0 = 0.2	e_0 = 0.4	e_0 = 0.8		e_0 = 0.2	e_0 = 0.4	e_0 = 0.8
(10^2, 5)	0.2	1.1454	1.2347	1.4637		1.1949	1.3583	1.9398
	0.4	0.9831	1.0462	1.1903		1.0232	1.1465	1.5508
	0.8	0.7191	0.7488	0.7939		0.7441	0.8060	0.9714
	1	0.6671	0.6904	0.7394		0.6887	0.7407	0.8827
(10^2, 10)	0.2	1.0627	1.1376	1.3221		1.1073	1.2481	1.7536
	0.4	0.8847	0.9343	1.0312		0.9202	1.0192	1.3283
	0.8	0.6354	0.6554	0.7213		0.6554	0.7011	0.8180
	1	0.5596	0.5753	0.6511		0.5766	0.6138	0.7247

The DMF sharply decreases by increasing the foundation supporting parameter and the foundation stiffness parameters, while it increases with the increase of the porosity coefficient, regardless of the porosity distribution type. The increase of the DMF by increasing the porosity coefficient e_0 is, however dependent on the foundation supporting parameter α_F, and this increase is less significant for the beam associated with a higher parameter α_F.

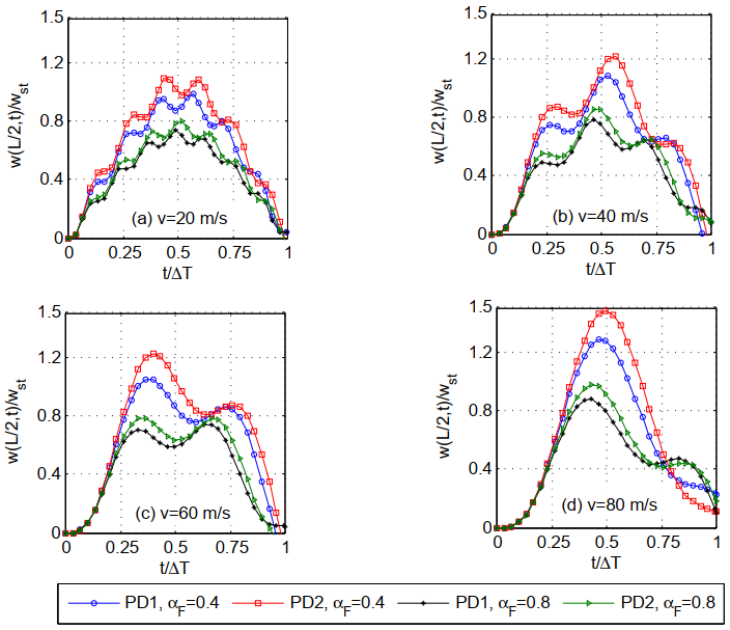

Figure 2. Time histories for mid-span deflection for L/h = 20, e_0 = 0.5, k_1 = 100, k_2 = 5 and different values of foundation supporting parameters and moving load velocity.

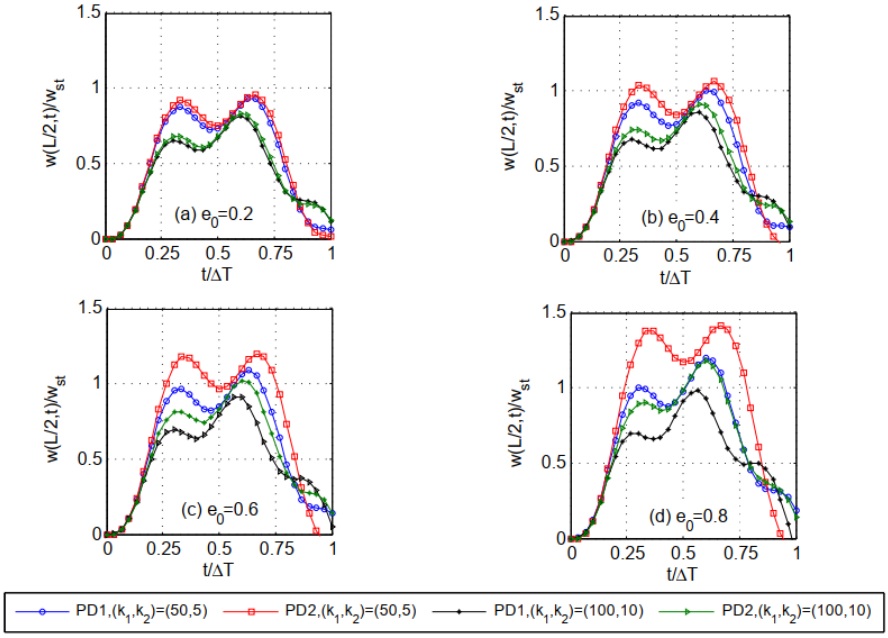

Figure 3. Time histories for mid-span deflection for L/h = 20, α_F = 0.5, v = 50 m/s and different values of foundation stiffness parameters and porosity coefficient.

In Figures 2 and 3, the time histories for mid-span deflection of both the DP1 and DP2 beams are shown for various values of the moving load velocity v, the supporting parameter α_F, the porosity coefficient e_0 and the foundation stiffness parameters k_1, k_2. It is evident from Fig. 2 that the mid-span deflection of the beam is significantly influenced by the load velocity v and the supporting parameter α_F as well. An increase in the parameter α_F leads to a decrease in the mid-span deflection, and the beam tends to perform fewer vibration cycles for a higher moving load velocity. The effect of the porosity coefficient and the foundation stiffness parameters on the time histories of the beam is clearly seen in Figure 3, where the mid-span deflection is seen to be decreased with increasing the foundation stiffness parameters and decreasing the porosity coefficient. Observation from these figures also shows that the mid-span deflections obtained from PD1 beam is always smaller than that obtained by PD2 beam. Thus, the PD2 has more impact on the dynamic response of the beam than the PD1 does.

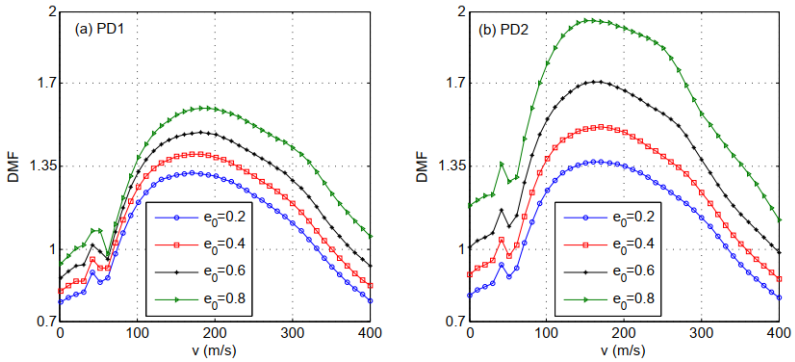

Figure 4. Variation of dynamic magnification factor with moving load velocity for L/h = 20, α_F = 0.5, (k_1, k_2) = (100, 5) and different porosity coefficients.

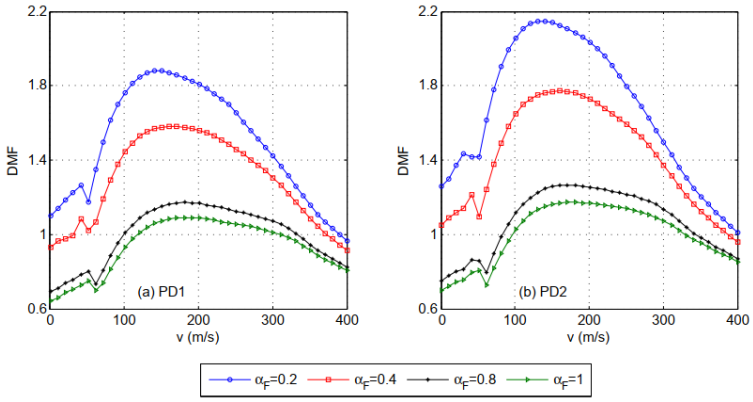

Figure 5. Variation of dynamic magnification factor with moving load velocity for L/h = 20, α_F = 0.5, (k_1, k_2) = (100, 5) and different foundation supporting parameters.

In Figures 4 and 5, the variation of the DMF with the moving load velocity of the FG porous beam associated with the two porosity distributions is depicted for different porosity coefficients and foundation supporting parameters, respectively. One can see from the figures that as in the case of the homogeneous beams under a moving load [30], the DMF repeatedly increases and decreases when increasing the moving load velocity v, it then reaches a maximum value. Besides, the relation between DMF and the moving load velocity is highly dependent on

the porosity coefficient and the foundation supporting parameter. The DMF increases by increasing the porosity coefficient (Figure 4), and it is lower for a higher foundation supporting parameter α_F (Figures 5). It can also be seen from Figures 4 and 5 that the maximum value of the dynamic magnification factor obtained by PD2 is always higher than that obtained by PD1, irrespective of the porosity coefficient and foundation supporting parameter. In other words, PD2 has a more impact on the dynamic response of the FG porous beam than PD1 does. In addition, the moving load velocity at which the DMF attains a maximum value is dependent on the porosity coefficient and the foundation supporting parameter as well.

Shown in Figures 6 and 7 are the variations of the DMF with the foundation stiffness parameters k_1 and k_2 for different porosity coefficients and the moving load velocities, respectively. The results in these figures depicted for both PD1 and PD2. As expected, the DMF decreases with the increase in the foundation stiffness parameters, regardless of the porosity coefficient and the moving load velocity. The difference between the dynamic response of the beam obtained by the two porosity distributions is clearly seen in the figure, and this difference is more significant for the beam with a higher porosity coefficient.

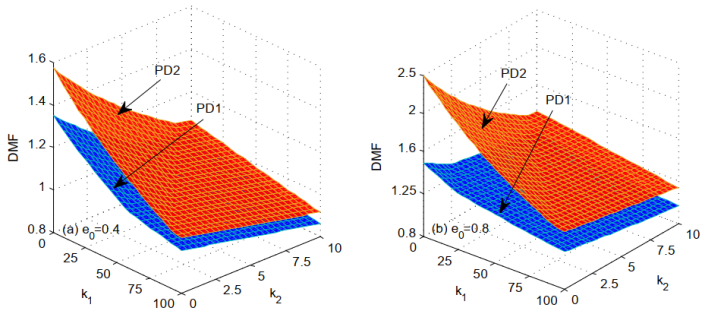

Figure 6. Variation of dynamic magnification factor of the FG porous beam with foundation stiffness parameters for L/h = 20, α_F = 0.5, v = 50 m/s and different porosity coefficients.

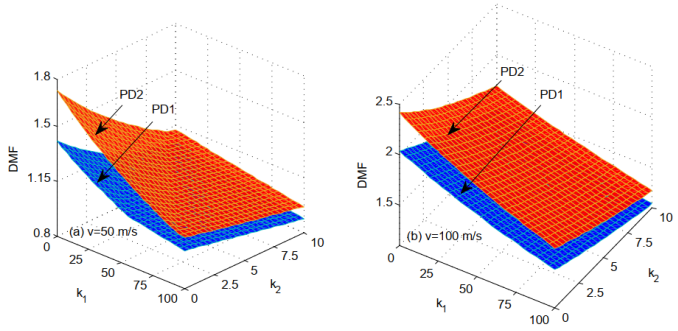

Figure 7. Variation of dynamic magnification factor of the FG porous beam with foundation stiffness parameters for L/h = 20, α_F = 0.5, e_0 = 0.5 and different moving load velocities.

Finally, the thickness distributions of the axial stress and the shear stress of the FG porous beam are respectively depicted in Figs. 8 and 9 for L/h = 20, α_F = 0.5, (k_1, k_2) = (100, 5), v = 50 m/s and four values of the porosity coefficient, e_0 = 0, 0.2, 0.4, 0.8. The stresses shown in the figures are obtained for both the two types of porosity distribution, and they are normalized as $\sigma^*_{xx} = \sigma_{xx}(L/2, z)/\sigma_0$, $\tau^*_{xz} = \tau_{xz}(0, z)/\sigma_0$ with $\sigma_0 = P/A$. One can see from Fig. 8 that the axial stress is linear distribution through the thickness for the non-porous beam (e_0 = 0), while it nonlinearly varies in the beam thickness for the FG porous beam.

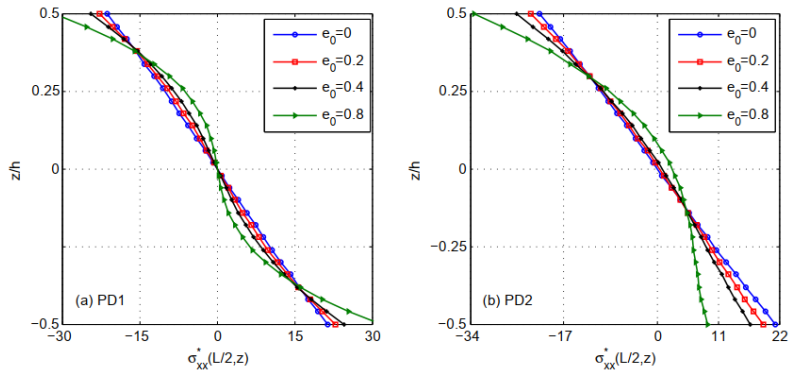

Figure 8. Thickness distribution of axial stress for L/h = 20, α_F = 0.5, (k_1, k_2) = (100, 5) and v = 50 m/s and different porosity coefficients.

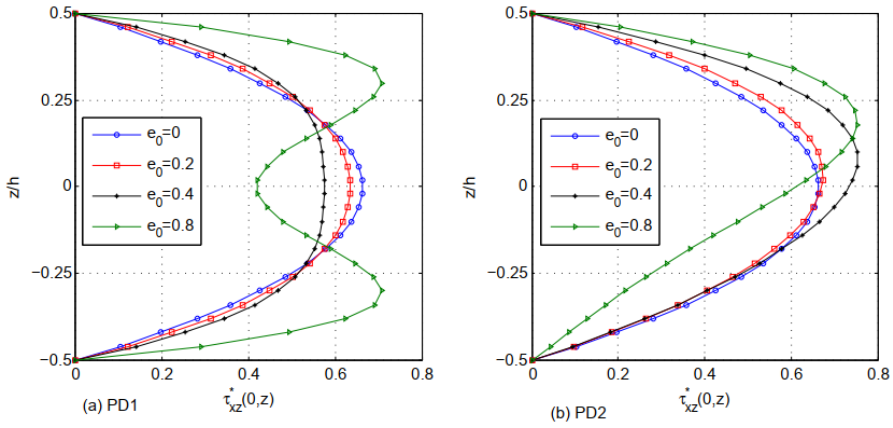

Figure 9. Thickness distribution of shear stress for L/h = 20, α_F = 0.5, (k_1, k_2) = (100, 5) and v = 50 m/s and different porosity coefficients.

The two porosity distribution types, as seen from Figure 8, have an opposite influence on the axial stress, and the maximum tensile stress of the PD1 beam increases by the increase of the coefficient e_0 (Figure 8a), while that of the PD2 beam decreases by increasing the coefficient e_0 (Figure 8b). Figure 9 shows a significant influence of the porosity distribution type on the shear stress distribution, where the thickness distribution of the shear stress of the PD2 beam (Figure 9b) is no longer symmetric as that of the PD1 beam (Figure 9a).

6. CONCLUSIONS

Dynamics of FG beams carrying of a moving load with the influence of porosities and partial support by a Pasternak foundation has been investigated. The beams made from an open-cell steel foam with two types of the porosity distribution, the symmetric and asymmetric distributions, are modelled in the basis of the refined third-order shear deformation theory. The discrete equation of motion for the beams is derived by using a two-node finite beam element, and it is solved by the Newmark method. Numerical investigation was carried out to study the

effects of the porosities, the foundation support and the moving load velocity on the dynamic behavior of the beams. The most important findings from the numerical results can be summarized as follows.

- The foundation supporting length plays an important role on dynamic response of FG porous beams, and the influence of the porosity coefficient on the dynamics is governed by the foundation supporting length.
- The increase of the DMF by increasing the porosity coefficient is dependent on the foundation supporting length, and this increase is less significant for the beam supported by a longer supporting foundation.
- Among the two types of porosity distribution, the PD1 has more impact on the dynamic response than the PD2 does, and the difference between the DMFs obtained by the two porosity distribution types is more significant for a higher porosity coefficient.

Declaration of competing interest. The author declares that she has no known competing financial interests or personal relationships that could have appeared to influence the work reported in this paper.

REFERENCES

1. Koizumi M. - FGM activities in Japan, Composites Part B: Engineering **28** (1-2) (1997) 1-4. https://doi.org/10.1016/S1359-8368(96)00016-9.
2. Şimşek M. and Kocaturk T. - Free and forced vibration of a functionally graded beam subjected to a concentrated moving harmonic load, Composite Structures **90** (4) (2009) 465-473. https://doi.org/10.1016/j.compstruct.2009.04.024.
3. Şimşek M. - Vibration analysis of a functionally graded beam under a moving mass by using different beam theories, Composite structures **92** (4) (2010) 904-917. https://doi.org/10.1016/j.compstruct.2009.09.030.
4. Khalili S. M. R., Jafari A. A. and Eftekhari S. A. - A mixed ritz-dq method for forced vibration of functionally graded beams carrying moving loads, Composite Structures **92** (10) (2010) 2497-2511. https://doi.org/10.1016/j.compstruct.2010.02.012.
5. Rajabi K., Kargarnovin M. H. and Gharini M. - Dynamic analysis of a functionally graded simply supported Euler-Bernoulli beam subjected to a moving oscillator, Acta Mechanica **224** (2) (2013) 425-446. https://doi.org/10.1007/s00707-012-0769-y.
6. Wang Y. and Wu D. - Thermal effect on the dynamic response of axially functionally graded beam subjected to a moving harmonic load, Acta Astronautica **127** (2016) 171-181. https://doi.org/10.1016/j.actaastro.2016.05.030.
7. Songsuwan W., Pimsarn M. and Wattanasakulpong N. - Dynamic responses of functionally graded sandwich beams resting on elastic foundation under harmonic moving loads, International Journal of Structural Stability and Dynamics **18** (9) (2018) 1850112. https://doi.org/10.1142/S0219455418501122.
8. Ga B. S., Trinh T. H., Le T. H. and Nguyen D. K. - Dynamic response of nonuniform timoshenko beams made of axially FGM subjected to multiple moving point loads, Structural Engineering and Mechanics **53** (5) (2015) 981-995.

9. Esen I. - Dynamic response of a functionally graded Timoshenko beam on two-parameter elastic foundations due to a variable velocity moving mass, International Journal of Mechanical Sciences **153** (2019) 21-35. https://doi.org/10.1016/j.ijmecsci.2019.01.033.
10. Esen I. - Dynamic response of functional graded Timoshenko beams in a thermal environment subjected to an accelerating load, European Journal of Mechanics-A/Solids **78** (2019), 103841. https://doi.org/10.1016/j.euromechsol.2019.103841.
11. Esen I., Eltaher M. A. and Abdelrahman A. A. - Vibration response of symmetric and sigmoid functionally graded beam rested on elastic foundation under moving point mass, Mechanics Based Design of Structures and Machines (2021) 1-25. https://doi.org/10.1080/15397734.2021.1904255.
12. Nguyen D. K., Nguyen Q. H., Tran T. T. and Bui V. T. - Vibration of bidimensional functionally graded Timoshenko beams excited by a moving load, Acta Mechanica **228** (1) (2017) 141-155. https://doi.org/10.1007/s00707-016-1705-3.
13. Nguyen D. K., Vu A. N. T., Le N. A. T. and Pham V. N. - Dynamic behavior of a bidirectional functionally graded sandwich beam under nonuniform motion of a moving load, Shock and Vibration **2020** (2020). https://doi.org/10.1155/2020/8854076.
14. Nguyen D. K., Vu A. N. T., Pham V. N. and Truong T. T. - Vibration of a threephase bidirectional functionally graded sandwich beam carrying a moving mass using an enriched beam element, Engineering with Computers **38** (2021) 1-12. https://doi.org/10.1007/s00366-021-01496-3.
15. Nguyen D. K., Tran T. T., Pham V. N. and Le N. A. T. - Dynamic analysis of an inclined sandwich beam with bidirectional functionally graded face sheets under a moving mass, European Journal of Mechanics-A/Solids **88** (2021) 104276. https://doi.org/10.1016/j.euromechsol.2021.104276.
16. Wattanasakulpong N. and Ungbhakorn V. - Linear and nonlinear vibration analysis of elastically restrained ends FGM beams with porosities, Aerospace Science and Technology **32** (1) (2014) 111-120. https://doi.org/10.1016/j.ast.2013.12.002.
17. Chen D., Yang J. and Kitipornchai S. - Free and forced vibrations of shear deformable functionally graded porous beams, International Journal of Mechanical Sciences **108** (2016) 14-22. https://doi.org/10.1016/j.ijmecsci.2016.01.025.
18. Ebrahimi F. and Jafari A. - A higher-order thermomechanical vibration analysis of temperature-dependent FGM beams with porosities, Journal of Engineering **2016** (2016). https://doi.org/10.1155/2016/9561504.
19. Ebrahimi F. and Jafari A. - Thermo-mechanical vibration analysis of temperature-dependent porous FG beams based on Timoshenko beam theory, Structural Engineering and Mechanics **59** (2) (2016) 343-371. https://dx.doi.org/10.12989/sem.2016.59.2.343.
20. Ebrahimi F. and Jafari A. - A four-variable refined shear-deformation beam theory for thermomechanical vibration analysis of temperature-dependent FGM beams with porosities, Mechanics of Advanced Materials and Structures **25** (3) (2018) 212-224. https://doi.org/10.1080/15376494.2016.1255820.
21. Ebrahimi F., Ghasemi F. and Salari E. - Investigating thermal effects on vibration behavior of temperature-dependent compositionally graded Euler beams with porosities, Meccanica **51** (1) (2016) 223-249. https://doi.org/10.1007/s11012-015-0208-y.

22. Atmane H. A., Tounsi A. and Bernard F. - Effect of thickness stretching and porosity on mechanical response of a functionally graded beams resting on elastic foundations, International Journal of Mechanics and Materials in Design **13** (1) (2017) 71-84. https://doi.org/10.1007/s10999-015-9318-x.
23. Akbaş Ş. D., Fageehi Y. A., Assie A. E. and Eltaher M. A. - Dynamic analysis of viscoelastic functionally graded porous thick beams under pulse load, Engineering with Computers (2020) 1-13. https://doi.org/10.1007/s00366-020-01070-3.
24. Jena S. K., Chakraverty S. and Malikan M. - Application of shifted Chebyshev polynomialbased RayleighRitz method and Naviers technique for vibration analysis of a functionally graded porous beam embedded in Kerr foundation, Engineering with Computers **37** (4) (2021) 3569-3589. https://doi.org/10.1007/s00366-020-01018-7.
25. Vu A. N. T., Le N. A. T. and Nguyen D. K. - Dynamic behaviour of bidirectional functionally graded sandwich beams under a moving mass with partial foundation supporting effect, Acta Mechanica **232** (7) (2021) 2853-2875. https://doi.org/ 10.1007/s00707-021-02948-z.
26. Fahsi B., Bouiadjra R. B., Mahmoudi A., Benyoucef S. and Tounsi S. - Assessing the effects of porosity on the bending, buckling, and vibrations of functionally graded beams resting on an elastic foundation by using a new refined quasi-3D theory, Mechanics of Composite Materials **55** (2) (2019) 219-230. https://doi.org/10.1007/s11029-019-09805-0.
27. Thai H, T. and Kim S. E. - A simple higher-order shear deformation theory for bending and free vibration analysis of functionally graded plates, Composite Structures **96** (2013) 165-173. https://doi.org/10.1016/j.compstruct.2012.08.025
28. Geradin M. and Rixen D. - Mechanical Vibrations, Theory and Application to Structural Dynamics, John Wiley & Sons, Chichester, 1997.
29. Song Q., Shi J. and Liu Z. - Vibration analysis of functionally graded plate with a moving mass, Applied Mathematical Modelling **46** (2017) 141-160. https://doi.org/10.1016/ j.apm.2017.01.073.
30. Olsson M. - On the fundamental moving load problem, Journal of Sound and Vibration **145** (2) (1991) 299-307. https://doi.org/10.1016/0022-460X(91)90593-9.